Detecting planetary-mass primordial black holes with resonant electromagnetic gravitational-wave detectors

Nicolas Herman ●,[1,*] André Fűzfa ●,[1,2,†] Léonard Lehoucq ●,[1,3,‡] and Sébastien Clesse ●[4,2,§]

[1]*Department of Mathematics and Namur Institute for Complex Systems (naXys),*
University of Namur, Rue Grafé 2, B-5000, Namur, Belgium
[2]*Cosmology, Universe and Relativity at Louvain, Institute of Mathematics and Physics,*
Louvain University, 2 Chemin du Cyclotron, B-1348 Louvain-la-Neuve, Belgium
[3]*Department of theoretical physics at the ENS Paris-Saclay, University of Paris-Saclay,*
avenue des Sciences, 91190, Gif-sur-Yvette, France
[4]*Service de Physique Théorique, Université Libre de Bruxelles (ULB),*
Boulevard du Triomphe, CP225, B-1050 Brussels, Belgium

The possibility to detect gravitational waves (GW) from planetary-mass primordial black hole (PBH) binaries with electromagnetic (EM) detectors of high-frequency GWs is investigated. We consider two patented experimental designs, based on the inverse Gertsenshtein effect, in which incoming GWs passing through a static magnetic field induce EM excitations inside either a TM cavity or a TEM waveguide. The frequency response of the detectors is computed for post-Newtonian GW waveforms. We find that such EM detectors based on current technology may achieve a strain sensitivity down to $h \sim 10^{-30}$, which generates an EM induced power of 10^{-10} W. This allows the detection of PBH binary mergers of mass around $10^{-5} M_\odot$ if they constitute more than 0.01 percent of the dark matter, as suggested by recent microlensing observations. We envision that this class of detectors could also be used to detect cosmological GW backgrounds and probe sources in the early Universe at energies up to the grand unified theory scale.

I. INTRODUCTION

Gravitational waves (GW), first introduced by Einstein in 1916 [1,2] as a linear regime of the field equations of general relativity, were directly detected for the first time in 2015 by the LIGO/Virgo Collaboration [3]. These ground-based detectors use laser interferometry techniques, but there also exist other detection strategies. Einstein's equivalence principle implies that all types of energies produce and experience gravity in the same way. The energy of electromagnetic (EM) radiation must therefore source gravity just like compact objects do and, the other way around, gravity (e.g., gravitational waves) can manifest itself in the physical characteristics of electromagnetic radiation. This is the basic principle behind the EM detection (or emission) of GWs.

The use of EM fields to both generate and detect GWs has actually been considered for decades, for instance based on the (inverse) Gertsenshtein effect [4] relying on the coupling between GWs and EM waves in the presence of a strong static magnetic field. However, the weakness

of this coupling makes any GW detection extremely challenging. Therefore, experimental efforts have mostly concentrated on ground-based detectors based on laser interferometry, probing a rather low frequency range (typically 1–10 kHz). But this technique is not suited for the detection of high-frequency GWs (HFGWs), EM-based detectors are more suited to detect them. Section II presents a short historic review of HFGW detectors that have been built or proposed. The interested reader will find more details about detection strategies and potential high-frequency sources in a recent review [5].

In this paper, we propose two novel patented [6] experimental designs of resonant high-frequency EM detectors, based on the inverse Gertsenshtein effect, operating at MHz or GHz frequencies and feasible with current technology. We numerically compute the EM signal produced by passing HFGWs and consider planetary-mass primordial black holes (PBHs) as their potential sources. The detectors are constituted by either a waveguide or a cavity immersed in a transverse static magnetic field. This outer magnetic field serves two purposes in our design. First, a proper (transverse) orientation of this field is mandatory to convert HFGWs into EM waves through the inverse Gertsenshtein mechanism. Second, the external magnetic field boosts the output signal through a resonance

*[*]nicolas.herman@unamur.be
[†]andre.fuzfa@unamur.be
[‡]leonard.lehoucq@ens-paris-saclay.fr
[§]sebastien.clesse@ulb.ac.be

mechanism on specific radiation modes that are excited by the passing HFGWs.

There exists a broad range of hypothetical astrophysical or cosmological sources of HFGWs with frequencies from kHz to THz (see Ref. [5] and references therein), such as exotic compact objects, PBHs, inflation, reheating, oscillons, cosmic strings and other topological defects, large curvature fluctuations, and phase transitions in the early Universe. Some sources produce transient signals, like the merging of compact objects, while cosmological sources typically induce a permanent stochastic GW background. In particular, HFGW detectors operating at MHz and GHz frequencies might probe new physics up to the scale of the grand unified theories.

In this paper, we focus on the particular case of transient signals from the merging of light (planetary-mass scale) PBHs. Their existence is still hypothetical but motivated by several recent observations, such as microlensing events towards the Galactic bulge, recently detected by OGLE [7,8] and suggesting that such PBHs may constitute between 1% and 10% of dark matter (DM). LIGO/Virgo observations provide additional motivations for the existence of PBHs in the stellar range [9–11] and a unified scenario with a wide mass distribution imprinted by the known thermal history of the Universe has been presented in Ref. [12]. PBHs may originate from the gravitational collapse of primordial inhomogeneities in the early Universe. Above a mass $m_{\mathrm{PBH}} \approx 10^{11}$ kg, their evaporation time through the Hawking-Bekenstein mechanism is much larger than the age of the Universe. Beyond these motivations, the GW waveform from PBH mergers is well known, which allows us to simulate the exact detector response. Our work therefore aims at paving the road towards an experimental realization of a HFGW detector with a good enough strain sensitivity, of order $h \sim 10^{-30}$, to detect various GW sources.

The paper is organized as follows. After reviewing previous proposals of EM-based HFGW detectors in Sec. II, in Sec. III we introduce the theory behind the Einstein-Maxwell system and the Gertsenshtein effects. Section IV applies the theory to the case of two detector designs based on a resonant waveguide and a cavity, in an external static magnetic field. Section V is devoted to the computation of the expected rate and signal from planetary-mass PBH mergers. In Sec. VI we gather these calculations to compute the expected signal in our detectors, in terms of frequency response and induced EM power, for different realistic designs and different PBH masses. Finally, we compute forecasted limits on the possible PBH abundance, for two possible binary formation channels (primordial binaries and tidal capture in clusters). We discuss our results and present some perspectives in the conclusion (Sec. VII).

II. BRIEF HISTORY OF ELECTROMAGNETIC AND HFGW DETECTORS

The use of EM fields to both generate and detect GWs has actually been considered for decades. While Weber [13] envisioned the importance of both the generation and detection of GWs as early as 1960, in 1962 Gertsenshtein [4] discovered a resonance mechanism allowing to produce GWs from EM waves in the presence of a strong static magnetic field. Later, in Refs. [14,15], this mechanism was studied in greater details using Einstein's equations, scattering theory, and Feynman perturbation techniques. Gertsenshtein's mechanism was applied to astrophysics by Zeldovich [16]. Grishchuk and Sazhin [17–19] then introduced purely electromagnetic generators of GWs, using transverse magnetic/electric (TM/TE) resonant cavities. They envisioned GW emission-reception laboratory experiments and concluded that they might be experimentally feasible [18,19], which would open the road to futuristic technologies based on GW physics [20]. Resonant cavities and EM waveguides were then considered as possible detectors of gravitational radiation, either emitted by natural or artificial sources [18–26].

Using EM detectors of GWs would allow to explore higher frequency ranges than with laser interferometry, typically from kHz to 100 GHz when using radio frequencies or from 100 GHz to THz when using microwaves. Investigations of electromagnetic GW detectors began in the 1970s [14,18,19,21–25,27]. Those detectors either make use of the conversion of GWs to photons [14], the excitation or modification of resonant modes of EM cavities and waveguides [18,19,21–25,28], the change of the polarization plane of an EM wave due to the passing GWs [27], or induced birefringence of the interior of the cavity [26]. More recently, Ejlli *et al.* [29] used available data from experiments designed for the detection of weakly interacting slim particles to set limits on the stochastic GW background through graviton-to-photon conversion in the ultrahigh-frequency band (above 1 THz). Bentley *et al.* [30] also proposed a method to reduce the noise of interferometric GW detectors at high frequency (kHz). Other types of HFGW detectors have been recently proposed [31,32,32–34], using optically trapped dielectric microspheres in a cavity, resonance between a graviton and a magnon that is based on the Dirac equation in a curved spacetime, or high-frequency phonon-trapping acoustic cavities.

III. EINSTEIN-MAXWELL SYSTEM AND THE GERTSENSHTEIN EFFECTS

The Einstein-Maxwell system models the interplay of gravitation and electromagnetism by the coupling of their respective field equations (in SI units[1]),

$$R_{\mu\nu} = \frac{8\pi G}{c^4} T_{\mu\nu}^{(\text{em})}, \tag{1}$$

$$\nabla_\mu F^{\mu\nu} = -\mu_0 J^\nu, \tag{2}$$

where

$$T_{\mu\nu}^{(\text{em})} = \frac{1}{\mu_0}\left(g^{\alpha\beta} F_{\mu\alpha} F_{\nu\beta} - \frac{1}{4} g_{\mu\nu} F_{\alpha\beta} F^{\alpha\beta}\right) \tag{3}$$

is the Maxwell stress-energy tensor, where $F_{\mu\nu} = \partial_\mu A_\nu - \partial_\nu A_\mu$ is the Faraday tensor of the electromagnetic field, $g_{\mu\nu}$ and A_μ are the metric and four-vector potential, ∇_μ is the covariant derivative with respect to $g_{\mu\nu}$, $R_{\mu\nu}$ is the Ricci tensor, and J^ν is the four-current density. In general relativity, the interplay between gravitation and electromagnetism is twofold: first, spacetime is curved by the energy of the electromagnetic field as ruled by Eq. (1), and second, at the same time the propagation of the electromagnetic field $F_{\mu\nu}$ is governed by the covariant Maxwell equations in curved spacetime [Eq. (2)]. For a small electromagnetic compactness $GE_{\text{EM}}/(c^4 L) \ll 1$, where E_{EM} is the EM energy stored in some physical system of length L, the gravitational sector of the system can be safely treated in the weak-field limit [35].

First, one can consider the gravitational perturbations arising from EM sources in the Einstein field equations. Considering EM configurations consisting in a superposition of a static field $F_{\mu\nu}^{(s)}$ and a varying one $F_{\mu\nu}^{(v)}$, the quadratic terms in Eq. (3) yield three general classes of electromagnetically induced gravitational perturbations around a Minkowski background,

$$g_{\mu\nu} = \eta_{\mu\nu} + c_{\mu\nu} + w_{\mu\nu} + h_{\mu\nu}, \tag{4}$$

where $\eta_{\mu\nu} = \text{diag}(-1, +1, +1, +1)$ is the Minkowski metric and $c_{\mu\nu}, w_{\mu\nu}, h_{\mu\nu} \ll 1$ represent the metric perturbations. In the above equation, (i) $c_{\mu\nu}$ represents the static gravitational field generated by some external static magnetic or electric field (from a coil or a capacitor) and arises from the quadratic term in $F_{\mu\nu}^{(s)}$ in Eq. (3), while (ii) $w_{\mu\nu}$ is a gravitational wave generated by the varying EM [for which the source is the quadratic term in $F_{\mu\nu}^{(v)}$ in Eq. (3)] and (iii) $h_{\mu\nu}$ is another gravitational wave generated by the coupling between the external static field $F_{\mu\nu}^{(s)}$ and some EM wave $F_{\mu\nu}^{(v)}$ [crossed terms in Eq. (3)]. The case (i) was studied in Ref. [35] but does not give rise to a GW since the outer EM field is static. Case (ii) was studied for light propagating pulses in Refs. [36,37] and in Refs. [17–19,38] for EM waves in resonant hollow cavities.[2] Case (iii)

actually corresponds to what is called the direct Gertsenshtein effect [4,16]. This Gertsenshtein effect is a wave resonance mechanism in which light passing through a region of uniform magnetic field, perpendicular to the direction of light propagation, produces GWs. A monochromatic EM wave leads to an outgoing GW of the same frequency. Electromagnetic generation of GWs is a very faint process, due to the extreme weakness of gravitational coupling. Indeed, the metric perturbations $h_{\mu\nu}$ produced through the Gertsenshtein mechanism have an amplitude of order

$$h_{\mu\nu} \sim \frac{4GB_0 E_0 L^2}{c^5 \mu_0}, \tag{5}$$

where L is the size of the region in which the magnetic field and the EM wave interact, and B_0 and E_0 are the amplitudes of the static magnetic and varying electric fields, respectively. To give an idea, in order to generate a strain $h \approx 10^{-21}$ with $B_0 \approx 10$ T and $E_0 \approx 1$ MV/m, one needs a truly astronomical size for the interacting region, $L \approx 10^6$ km. Therefore, while the direct Gertsenshtein effect can be used to build electromagnetic GW generators, its practical application constitutes an extreme experimental challenge.

Second, ripples in spacetime can also interact with a static magnetic field to produce an outgoing EM wave. This inverse Gertsenshtein effect is described by the Maxwell equations (2) on a perturbed background. An obvious application of this effect is the detection of GWs passing into a transverse static magnetic field, GWs will be converted into EM waves. One possible way to derive the equations governing the inverse Gertsenshtein effect is to develop the covariant derivative in Eq. (2) at first order in metric perturbations, and to treat these as an effective current density. We follow here a different approach, based on a covariant generalization of the EM wave equations,[3]

$$g^{\alpha\beta}\nabla_\alpha\nabla_\beta F_{\mu\nu} + R_{\mu\nu\alpha\beta}F^{\alpha\beta} + R^\alpha{}_\mu F_{\nu\alpha} + R^\alpha{}_\nu F_{\alpha\mu} = 0, \tag{6}$$

where $R_{\mu\nu\alpha\beta}$ is the Riemann tensor. This set of equations describes the propagation of EM waves on a curved spacetime. In the case of a flat Minkowski spacetime, the wave equation (6) reduces to the classical wave equation $g^{\alpha\beta}\nabla_\alpha\nabla_\beta F_{\mu\nu} = 0$.

Let us now consider a small perturbation $h_{\mu\nu}$ propagating on a Minkowski background, such that the metric is given by $g_{\mu\nu} = \eta_{\mu\nu} + h_{\mu\nu}$ at first order ($h_{\mu\nu} \ll 1$). If this perturbation satisfies the Lorenz gauge condition, $\partial_\mu h^{\mu\alpha} = 0$, one gets from Eq. (6) the linearized wave equation for the Faraday tensor (see also Ref. [19]),

---

[2] In Ref. [17], a special case of a hollow spherical cavity in an outer radial magnetic field was briefly considered, giving rise to an admixture of terms $w_{\mu\nu}$ [case (ii)] and $h_{\mu\nu}$ [resonance—case (iii)] which were not identified as such nor exploited by the authors.

[3] These are obtained from the two groups of covariant Maxwell equations $\nabla_\mu F^{\mu\nu} = 0$ and $\nabla_\kappa F_{\mu\nu} + \nabla_\mu F_{\nu\kappa} + \nabla_\nu F_{\kappa\mu} = 0$, which can be combined to retrieve Eq. (6).

$$
\begin{aligned}
g^{\alpha\beta}\nabla_\alpha\nabla_\beta F^{(1)}{}_{\mu\nu} = {}& h^{\alpha\kappa}\nabla^{(\eta)}_\alpha\nabla^{(\eta)}_\kappa F^{(0)}{}_{\mu\nu} \\
& - \partial_\rho(\partial_\mu h_{\alpha\nu} - \partial_\nu h_{\alpha\mu})F^{(0)\rho\alpha} \\
& - (\partial^\gamma h^{\alpha\beta} + \partial^\alpha h^{\beta\gamma} - \partial^\beta h^{\gamma\alpha}) \\
& \times (\eta_{\alpha\mu}\nabla^{(\eta)}_\gamma F^{(0)}{}_{\nu\beta} - \eta_{\alpha\nu}\nabla^{(\eta)}_\gamma F^{(0)}{}_{\mu\beta}) = S_{\mu\nu}.
\end{aligned}
\tag{7}
$$

In the above equation, we have assumed that the total EM field $F_{\mu\nu}$ is the superposition of some background EM field $F^{(0)}{}_{\mu\nu}$ with which the metric perturbation $h_{\mu\nu}$ interacts to produce an EM perturbation $F^{(1)}{}_{\mu\nu}$. In the following, we focus on the magnetic conversion of GWs into photons, i.e., the interaction between a passing GW and an external static magnetic field ($F^{(0)}{}_{\mu\nu}$ is purely magnetic) which results in an EM wave emission. Equation (7) governs the inverse Gertsenshtein effect.

Under the assumption of a uniform static magnetic field, the first and third source terms in Eq. (7), both including $\nabla^{(\eta)}_\gamma F^{(0)}{}_{\alpha\beta}$, identically vanish, leaving as the only source term the one with second derivatives of the metric perturbations,

$$
S_{\mu\nu} = -\partial_\alpha(\partial_\mu h_{\beta\nu} - \partial_\nu h_{\beta\mu})F^{(0)\alpha\beta}.
\tag{8}
$$

We can now apply this theory and conceive a specific experiment for the detection of HFGWs produced, e.g., by inspiraling PBHs.

IV. RESONANT ELECTROMAGNETIC DETECTORS OF HFGWs

In this section, we describe two detector designs that are based on the patents in Ref. [6]. The detection principle is based on the inverse Gertsenshtein effect, and thus a passing GW interacts with an intense static magnetic field. If the direction of the incoming GW is not collinear with the magnetic field, faint transverse EM waves are generated and these can be further amplified by EM resonators. The experimental setup consists of either a waveguide or a cavity whose axis of symmetry is orthogonal to the magnetic field. Such a setup is similar to haloscopes that are used for the search for axions, like the ADMX experiment [39,40], except for the orientation of the outer magnetic field. As shown below, it is mandatory that it is orthogonal to the axis of the cavity/waveguide in order to detect GWs.

A theorem by Choquet-Bruhat [41] established that both direct and inverse Gertsenshtein effects require the condition of orthogonality between the external EM field and the direction of GW propagation. This theorem starts from the hypothesis that incoming or generated GWs have a Wentzel-Kramers-Brillouin form and are of high frequencies. The equation of propagation in Ref. [41] is then obtained after a development in frequency. We propose

below a variant of Choquet-Bruhat's demonstration with a development in the amplitude instead of frequency. We first assume that the incoming GW is a plane wave, $h_{\mu\nu} = a_{\mu\nu}e^{i\omega\Phi}$, with a general varying phase, $\Phi = \Phi(x^\alpha)$. The goal is to show that the constant EM field must be orthogonal to the direction of propagation of the incoming plane wave, in order to produce an EM wave. In other words, no EM wave can be generated from the interaction between a constant EM field and a GW, unless the first one is orthogonal to the direction of propagation of the second one. In order to show this, we demonstrate that a vanishing source term $S_{\mu\nu} = 0$ in Eq. (7) is equivalent to the condition $\Phi_\alpha F^{\alpha\mu(0)} = q\Phi^\mu$, where q is a real constant and $\Phi_\alpha = \partial_\alpha\Phi$. Since we assume that $E^{(0)}$ and $B^{(0)}$ are constants in our problem, the source term is given by Eq. (8). Therefore, the nonzero part of $S_{\mu\nu}$ is the exterior derivative of an effective four-current density: $J^{\text{eff}}_\mu = \partial_\alpha h_{\beta\mu}F^{\alpha\beta(0)}$. We can thus rewrite our source term as

$$
\begin{aligned}
S_{\mu\nu} &= \partial_\nu J^{\text{eff}}_\mu - \partial_\mu J^{\text{eff}}_\nu \\
&= (\Phi_\nu J^{\text{eff}}_\mu - \Phi_\mu J^{\text{eff}}_\nu)' \quad \text{with} \quad (\cdot)' \equiv \partial(\cdot)/\partial\Phi.
\end{aligned}
$$

The last line is obtained as a result of the plane-wave approximation (the amplitude $a_{\mu\nu}$ above is constant), which implies that the partial derivative ∂_ν is equivalent to $\Phi_\nu\frac{\partial}{\partial\Phi}$. Because a GW verifies the eikonal $\Phi_\mu\Phi^\mu = 0$ (if not, it is inconsistent and vanishes with a change of coordinate [41]), multiplying the above expression by Φ^μ gives that $S_{\mu\nu} = 0 \Leftrightarrow \Phi^\mu J^{\text{eff}}_\mu = 0$, and thus Φ_ν is orthogonal to J^{eff}_μ. Since Φ_μ does not vanish, this yields the equivalence $S_{\mu\nu} = 0 \Leftrightarrow J^{\text{eff}}_\mu = 0$. Let us now show the central result

$$
S_{\mu\nu} = 0 \Leftrightarrow J^{\text{eff}}_\mu = 0 \Leftrightarrow \Phi_\alpha F^{\alpha\mu(0)} = q\Phi^\mu.
\tag{9}
$$

For plane waves $h_{\mu\nu} = a_{\mu\nu}e^{i\omega\Phi(x^\alpha)}$, we have that $\partial_\alpha h_{\lambda\nu} = \Phi_\alpha h'_{\lambda\nu}$. Therefore, the effective four-current can be simplified to

$$
J^{\text{eff}}_\nu = F^{\alpha\lambda(0)}\Phi_\alpha h'_{\lambda\nu}
$$

If $\Phi_\alpha F^{\alpha\mu(0)} = q\Phi^\mu$, then $J^{\text{eff}}_\nu = q\Phi^\lambda h'_{\lambda\nu}$. In the meantime, the Lorenz gauge condition, $\partial^\mu h_{\mu\nu} = 0$, is equivalent to $\Phi^\mu h'_{\mu\nu} = 0$ in the plane-wave approximation. So we can conclude that the effective four-current density J^{eff}_ν vanishes. Now, let us prove the implication in the reverse way.

Let us assume $J^{\text{eff}}_\nu = 0$ and move to radiative coordinates, that is to say, $\Phi = x^0$ so we have directly $\Phi_0 = 1$ and $\Phi_i = 0$. The GW obey to the eikonal, so the time-components of the Minkoswki metric are $\eta^{00} = 0$ and $\eta^{0i} = \Phi^i$. In such a comobile coordinate system, the significant components of the wave are the h_{ij}. The source term becomes

$$J_\nu^{\mathrm{eff}} = \Phi_0 F^{0\lambda(0)} h'_{\lambda\nu} + \Phi_i F^{i\lambda(0)} h'_{\lambda\nu}$$
$$= F^{0\lambda(0)} h'_{\lambda\nu}$$
$$= F^{0j(0)} h'_{ij}.$$

So, the fact that $J_\nu^{\mathrm{eff}} = 0$ implies that $F^{0j(0)} h'_{ij} = 0$. At any point of spacetime, we can choose a spatial coordinate system such that $F^{0j(0)} = A\delta_1^j$. Then, we have $F^{0j(0)} h'_{ij} = 0$, which leads to $Ah'_{i1} = 0$, and so $A = 0$ since the GW is nonzero. Thus, $F^{0j(0)} = 0 = q\Phi^j$, because $\Phi^j = \eta^{0j} = 0$. Knowing that $\Phi_0 = 1$ and $\Phi_i = 0$, we can show that $F^{0j(0)} = \Phi_\alpha F^{\alpha j(0)}$. We can also consider that $\Phi^0 = 0$ and $F^{\alpha 0} = -F^{0\alpha}$ to conclude that $\Phi_\alpha F^{\alpha\mu(0)} = q\Phi^\mu$. This completes our demonstration. Let us now particularize the final result $\Phi_\alpha F^{\alpha\mu(0)} = q\Phi^\mu$ in an illustrative case. In Cartesian coordinates, we can write down the null vector $\Phi_\alpha = (k, 0, 0, k)$, where k is the wave vector of the incident GW which is therefore propagating along the z direction. The above-mentioned condition (9) now leads to two constraints on the EM field: $E^x + B^y = 0$ and $E^y - B^x = 0$. If one considers the case when there is no electric field, this condition implies that the components of the outer magnetic field that are transverse to the direction of GW propagation vanish: $B^x = B^y = 0$. In other words, any longitudinal magnetic field B^z does not produce any EM wave via the inverse Gertsenshtein effect (since $S_{\mu\nu} = 0$). To produce GWs by this mechanism, one needs $S_{\mu\nu} \neq 0$ or, equivalently, a nonvanishing magnetic field in the direction transverse to the GW propagation ($B_\perp \neq 0$).

This is the reason why experiments like ADMX [39] do not have the right configuration to detect GWs. Indeed, they use a longitudinal outer magnetic field which can therefore only interact with GWs propagating transversely to it. This interaction can only produce EM waves that are in the same direction as the constant magnetic field, but this is forbidden in the TM cavity they are using (since only transverse excitation modes are allowed, not longitudinal ones). To turn a haloscope into a HFGW detector, one simply needs to rotate the outer magnetic field by a quarter of a turn.

Let us now present our proposed experimental setups. One can either consider the resonance of the induced EM waves inside a cylindrical cavity of radius R or inside a waveguide made of two (or more) concentric open cylinders with inner radius R_1 and outer radius R_2. We denote by L the length of the resonators and by $B_{\mathrm{ext}}^{(0)}$ the external magnetic field, which is assumed to be of constant magnitude for simplicity. A schematic representation of our cavities can be found in Fig. 1.

We briefly present here the responses of these cavities to an incoming GW signal. The interested reader will find the details of the computations at the end of this paper, in the Appendix. In the following, we assume $c = 1$. The starting point is the induction of EM waves when the GW passes
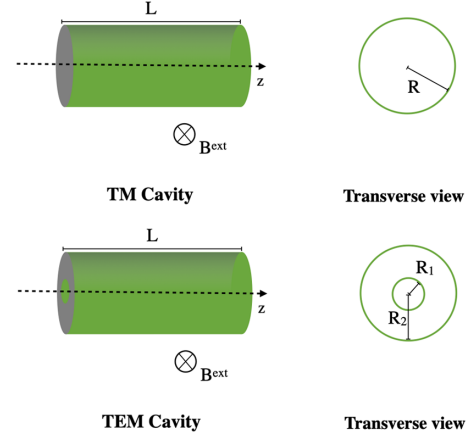

FIG. 1. Schematic representation of the experimental designs: a cylindrical TM cavity (top) and TEM waveguide (bottom), in an external static and transverse magnetic field.

perpendicularly to the static magnetic field, as described by Eq. (7). Considering the outer magnetic field along the x direction, $\vec{B}_{\mathrm{ext}}^{(0)} = B_{\mathrm{ext}}^{(0)} \vec{e}_x$, we obtain the following wave equation for the induced magnetic field $\vec{B}^{(1)}$:

$$\left(-\frac{\partial^2}{\partial t^2} + \vec{\Delta}\right)\vec{B}^{(1)} = B_{\mathrm{ext}}^{(0)} \begin{pmatrix} \frac{\partial^2 h_+}{\partial z^2}\cos(\phi) + \frac{\partial^2 h_\times}{\partial z^2}\sin(\phi) \\ -\frac{\partial^2 h_+}{\partial z^2}\sin(\phi) + \frac{\partial^2 h_\times}{\partial z^2}\cos(\phi) \\ 0 \end{pmatrix},$$
(10)

where h_+ and $h_\times$ are the usual polarizations of the incoming GW in the traceless-transverse gauge. Although there is also an induced electric field $\vec{E}^{(1)}$, the response of the detector is dominated by the induced magnetic field, as we shall see below.

We can then project Eq. (10) onto the proper functions of the Laplacian operator in cylindrical coordinates. This spectral decomposition is given by

$$B_{r,\phi}^{(1)}(t, r, \phi, z) \approx \sum_{k,m,n} \hat{b}_{k,m,n}^{r,\phi}(t) \cdot \psi_{kmn}^{r,\phi}(r, \phi, z), \quad (11)$$

where $\psi_{kmn}^{r,\phi}(r, \phi, z)$ are the cylindrical harmonics that satisfy the boundary conditions of our EM cavities. The result of this spectral decomposition allows to reduce the above wave equation (10) to an ordinary differential equation describing a forced harmonic oscillator for each spectral mode $\hat{b}_{k,m,n}^{r,\phi}$ in our cavity:

$$\frac{d^2 \hat{b}_{k,m,n}^{r,\phi}}{dt^2} + \Omega_{kn}^2 \hat{b}_{k,m,n}^{r,\phi} = \hat{s}_{k,m,n}^{r,\phi}(t), \quad (12)$$

where Ω_{kn}^2 are the proper frequencies of the resonant cavities and $\hat{s}_{k,m,n}^{r,\phi}(t)$ are the spectral coefficients of the source of the wave equation (10).

The energy variation $\Delta\mathcal{E}$ inside the cavity is given at the leading order by (see the Appendix for details)

$$\Delta\mathcal{E} \approx \frac{2\pi B_0}{\mu_0} \cdot \sum_k \mathcal{I}_k \hat{b}_{k,1,0}(t), \qquad (13)$$

where the coefficients $\mathcal{I}_k$ arise from the spatial averaging in the transverse directions (these adimensional quantities depend on the cavity geometry only). Let us recall that the numbers k, m label the transverse decomposition in the radial and azimuthal directions, while the number n labels the different longitudinal modes. We can see that only the $(k, 1, 0)$ modes, which are constant in the longitudinal direction z (since $n = 0$), contribute to the energy variation at first order in $B^{(1)}$. Since these $(k, 1, 0)$ modes do not propagate along z, one can see that there is no spatial phase shift with this energy variation at first order. These $(k, 1, 0)$ modes of the induced magnetic field are sourced by

$$\hat{s}_{k,1,0}^{r,\phi}(z, t) = \pi B_0 L^2 \mathcal{I}_k \int_{-L/2}^{L/2} \frac{\partial^2 h_+(z, t)}{\partial z^2} \, dz. \qquad (14)$$

The detailed computations from Eq. (7) to Eqs. (12)–(14) are available at the end of this paper, in the Appendix.

A dimensional analysis of Eq. (13) leads to the following estimation for the order of magnitude of the induced energy variation inside the resonator:

$$\Delta\mathcal{E} \approx \frac{2\pi B_0^2 L^3}{\mu_0} \mathcal{H}_{\mathrm{GW}} \mathcal{F}, \qquad (15)$$

where $\mathcal{H}_{\mathrm{GW}}$ is the (dimensionless) amplitude of the strain of the GW and $\mathcal{F}$ is an adimensional geometrical factor[4] accounting for the shape of the resonator (length and diameter). This factor $\mathcal{F}$ is of the order of unity when the spectrum of the incoming GW matches the resonance bandwidth. In the other cases, we must consider a frequency-dependent geometrical factor $\mathcal{F}(\omega)$.

Please note that with our model there is no temporal phase shift in the conversion process. Indeed, there is no imaginary part in the Fourier transform of ΔE and so the complex argument is null. This is mainly due to the fact that Eq. (12) is purely harmonic, without any dissipation, and therefore no phase shift can happen. Instead of a derivation in the time domain, one could also use a frequency approach of the cavity responses to demonstrate this, but this goes beyond the scope of this paper. However, the ohmic losses of energy in the sidewalls of the cavities could be represented by a dissipative term in Eq. (12), and so a phase shift could appear in the conversion process for resistive cavities. Although ohmic losses will lower the

efficiency of the resonance mechanism investigated here, this can be avoided by working with superconducting cavities.

V. HFGWs FROM PLANETARY-MASS PRIMORDIAL BLACK HOLE MERGERS

PBH binaries may have formed through two different channels: first, in the early Universe, when two PBHs form sufficiently close to each other for their dynamics to decouple from the expansion of the Universe, before the matter-radiation equality [11,42]; second, by tidal capture in dense environments [9,10], such as ultra-faint dwarf galaxies. In this section, we review the motivations to consider planetary-mass PBHs binaries and we estimate their expected merging rate and gravitational-wave signal, for these two channels. We then calculate the astrophysical range of resonant electromagnetic detectors as a function of their strain sensitivity. Finally, we compute for each formation channel the limits that could be set on the abundance of planetary-mass PBHs.

A. Motivations

The progenitor masses and low effective spins of the black hole mergers detected by LIGO/Virgo have revived the interest for PBHs in the $[1\text{–}100] \, M_\odot$ range [9–11,43]. However, it is debated if PBHs could constitute only a small fraction, or up to the totality of the DM in the Universe. In this context, detecting a subsolar black hole would almost clearly point to a primordial origin.[5] Going beyond the simplest but unrealistic assumption of a monochromatic mass function, the distribution of PBHs could span several decades of masses, as is the case if curvature fluctuations at the origin of PBH formation are nearly scale invariant—a generic prediction of inflation— or come from a broad peak in their power spectrum. Then, the known thermal history of the Universe, in particular the QCD transition at ~ 100 MeV and the electroweak epoch at ~ 100 GeV, should have left imprints in the PBH mass function [12,46], even if we do not know the mechanism at the origin of these curvature fluctuations. These features take the form of a high peak at the solar mass scale and two bumps at $\sim 30 \, M_\odot$ and $\sim 10^{-5} \, M_\odot$. Such an extended mass function could explain a series of puzzling observations (see Refs. [12,47] and references therein) such as unexpected microlensing events, LIGO/Virgo black hole mergers, some properties of ultra-faint dwarf galaxies, unexpected correlations in x-ray and infrared cosmic backgrounds, and supermassive black holes at high redshifts. The bump in the planetary-mass range is consistent with recent detections of star and quasar microlensing

---

[4]In other words, we extract all of the dimensional factors in Eq. (13), leaving just one adimensional expression that depends on the geometry of the detector and its frequency sensitivity.

[5]However, see Refs. [44,45] for another subsolar black hole formation channel, with different spin predictions, in a specific dark matter scenario.

events [7,48,49], which suggest a DM fraction of $f_{PBH} \sim 0.01$ made of compact objects, quite much more than one can expect for floating planets, but that could be expected for PBHs in the unified scenario presented in Ref. [12]. Recently, the possible detection of a stochastic GW background at nHz frequencies by NANOGrav [50] may also hint at the existence of PBHs with planetary [51] or stellar [52–54] masses, and Wang *et al.* [55,56] put some constraints on the PBH abundance for the current detectors to probe a stochastic GW background made of PBHs. However, all of these observations could have another origin and the derived limits are still subject to large astrophysical uncertainties. In the future, it is therefore important to find complementary ways to probe the existence of such objects, and to distinguish their nature and origin.

As we show in this paper, HFGW detectors will have the ability to detect or set new limits on the abundance of light, subsolar PBHs, of mass $m_{PBH} \sim 10^{-5} M_\odot$. HFGWs are indeed produced during the merging phase of such light PBHs. The frequency associated with the innermost stable circular orbit (ISCO), when the GW emission is close to maximal, is given by

$$f_{ISCO} = \frac{4400 \text{ Hz}}{(m_1 + m_2)/M_\odot}, \qquad (16)$$

where m_1 and m_2 are the masses of the two binary components. A frequency of 200 MHz thus corresponds to a PBH mass of $10^{-5} M_\odot$, the same order as the mass of the lenses at the origin of the microlensing events reported in Ref. [7]. Nevertheless, for being an interested HFGW signal, one needs to investigate if the merging rate of such PBHs can lead to at least $\mathcal{O}(1)$ mergers per year within the HFGW detector range.

PBHs therefore constitute a target of much interest for our experimental concept of EM detection of HFGWs. From the amplitude and spectral response of the resonant detectors, we will characterize the expected signals from PBH mergers for a large range of progenitor masses in the interval $[10^{-8}; 10^{-3}] M_\odot$, located at 1 Gpc distance. Then, for a given detector sensitivity, we will compute the expected limits on the PBH abundance.

B. Gravitational waves from inspiraling binaries

A good estimation of the GW strain produced at a given frequency f_{GW} during the inspiraling phase of a black hole binary is provided by the post-Newtonian approximation [57],

$$h \approx \frac{2}{D} \left(\frac{G\mathcal{M}}{c^2} \right)^{5/3} \left(\frac{\pi f_{GW}}{c} \right)^{2/3}, \qquad (17)$$

where $\mathcal{M} \equiv (m_1 m_2)^{3/5}/(m_1 + m_2)^{1/5}$ is the binary chirp mass and D is the distance to the observer. The GW

emission is close to maximal at the ISCO frequency and, for a given chirp mass, for equal mass binaries, $m_1 = m_2 = m_{PBH}$. For an experiment with a detector strain sensitivity h_{det} at this maximal frequency, the corresponding astrophysical reach D_{max} is given by

$$D_{max} \approx 1.6 \times \frac{(m_{PBH}/M_\odot)}{h_{det} \times 10^{20}} \text{ Mpc}. \qquad (18)$$

For instance, for a strain sensitivity of $h_{det} \sim 10^{-25}$ and $m_{PBH} \sim 10^{-5} M_\odot$, eventual mergers towards the Galactic center, in the Milky Way DM halo, or in satellite ultra-faint dwarf galaxies, could be detected. For a better sensitivity down to $h_{det} \sim 10^{-30}$, corresponding to the optimal sensitivity of the proposed designs of resonant EM detectors, one would probe planetary-mass PBH mergers in more distant galaxies.

C. Merging rate of primordial binaries

If PBHs are spatially randomly distributed at formation, it happens that two PBHs form so close to each other that their gravitational attraction overpasses the effect of the Hubble-Lemaître expansion at some point before matter-radiation equality. In such a case, they directly form a binary whose orbital parameters and lifetime depend not only on the two black hole masses but also on the mass and distance of the nearest PBHs. Eventually, it takes of the order of the age of the Universe for the PBH binary to merge. The merging rates τ today associated with this binary formation channel and an arbitrary mass function have been evaluated in Refs. [58–61] as

$$\begin{aligned} R^{prim}(m_1, m_2) &\equiv \frac{d\tau}{d \ln m_1 d \ln m_2} \\ &\approx \frac{1.6 \times 10^6}{\text{Gpc}^3 \text{ yr}} f_{PBH}^2 f(m_1) f(m_2) f_{sup} \\ &\times \left(\frac{m_1 + m_2}{M_\odot} \right)^{-\frac{32}{37}} \left[\frac{m_1 m_2}{(m_1 + m_2)^2} \right]^{-\frac{34}{37}}, \end{aligned} \qquad (19)$$

where $f(m)$ is the today density distribution of PBHs normalized to one ($\int f(m) d \ln m = 1$) and f_{PBH} is the integrated DM fraction made of PBHs. We also define an effective parameter

$$\tilde{f}_{PBH}(m_{PBH}) \equiv f_{PBH} f(m_{PBH}) f_{sup}^{1/2} \qquad (20)$$

that includes a rate suppression factor (f_{sup}) to take into account the possible rate suppression due to binary disruption by early-forming clusters, an effect put in evidence by N-body simulations when $f_{PBH} \gtrsim 0.1$ [62]. In such a case, one can recover the LIGO/Virgo merging rates inferred from the recent detections of GW190425, GW190521, and GW190814 involving at least one BH in

the mass gaps, with $f_{PBH} = 1$ and $f_{sup} \simeq 0.0025$ [63]. In the opposite case, $f_{sup} = 1$ and $\tilde{f}_{PBH}$ simply represents the DM density fraction made of PBHs at a given mass and within a unit logarithmic mass interval.

If one considers the merging rates of equal-mass binaries that produce the largest strain signal, one gets

$$R^{prim}(m_{PBH}) \approx \frac{3.1 \times 10^6}{Gpc^3 \, yr} \tilde{f}_{PBH}^2 \left(\frac{m_{PBH}}{M_\odot}\right)^{-0.86}. \quad (21)$$

In turn, one can determine the radius of the sphere in which one expects one event per year,

$$D_1^{prim} = \left(\frac{4\pi}{3} R^{prim}\right)^{-1/3}$$

$$\approx 4.2 \text{ Mpc} \times \tilde{f}_{PBH}^{-2/3} \left(\frac{m_{PBH}}{M_\odot}\right)^{0.29}. \quad (22)$$

For simplicity we neglected the effects of redshift, which are anyway insignificant for most of the considered cases. For instance, in the scenario of Refs. [12,63] with $f_{PBH} = 1$, $f_{sup} = 0.0025$, and $f(10^{-5} M_\odot) \simeq 10^{-2}$, one gets $D_1^{prim}(10^{-5} M_\odot) \approx 23$ Mpc. Using Eqs. (17) and (18), one then obtains the required GW strain sensitivity to detect one of these merger events per year,

$$h_1^{prim} \approx 3.8 \times 10^{-21} \tilde{f}_{PBH}^{2/3} \left(\frac{m_{PBH}}{M_\odot}\right)^{0.7} \quad (23)$$

$$\approx 8.3 \times 10^{-19} \tilde{f}_{PBH}^{2/3} \left(\frac{Hz}{f}\right)^{0.7}, \quad (24)$$

which can be typically targeted by GW experiments detecting frequencies from kHz up to GHz. This relation can be inverted to obtain a limit on the DM fraction at a given mass (if $f_{PBH} < 0.1$) in the case of null detection, as a function of the strain sensitivity,

$$\tilde{f}_{PBH} \lesssim 9.1 \left[\frac{h_{det}}{10^{-20}}\right]^{3/2} \left(\frac{m_{PBH}}{M_\odot}\right)^{-1.07}. \quad (25)$$

However, the strain sensitivity of the detector depends on the waveform and signal duration, which depend on the PBH mass. It is thus more adequate to compute a limit on the PBH abundance taking these effects into account and instead assuming an EM power sensitivity, which we do in the next section. For instance, with the two proposed experimental designs and a power sensitivity of 10^{-10} W, we obtain limits that are competitive with the current microlensing limits at the same mass scale. These are represented in our final Fig. 7.

Finally, we point out that when our analysis was being finalized, the authors of Ref. [64] claimed that the rates from primordial binaries are highly suppressed compared to previous calculation. The reason is a subtle general-relativistic effect arising when one considers geodesics in black hole exterior spacetime metrics that are Friedmann-Lemaître-Robertson-Walker asymptotic. If this claim is correct, primordial binaries are by far outside the reach of EM detectors, but one can nevertheless consider the merging rates inside PBH clusters, which we detail below.

D. Merging rate from PBH clusters

The second binary formation channel is through dynamical capture in dense PBH halos. Like any other DM candidate, PBHs are expected to form halos during the cosmic history, and their clustering properties determine the overall merging rate. For instance, for a monochromatic mass spectrum and a standard Press-Schechter halo mass function, one gets a rate [9]

$$R^{capt} \sim f_{PBH}^2 \times \mathcal{O}(1\text{--}100) \text{ yr}^{-1} \text{ Mpc}^{-3} \quad (26)$$

that is independent of the PBH mass. For more realistic extended mass functions, the abundance, size, and evolution of DM halos, partially or entirely made of PBHs, is impacted by several effects; see, e.g., Refs. [65–75]. Let us mention a Poissonian noise from the discrete nature of PBHs, a seeding effect from heavy PBHs, the enhancement of the primordial power spectrum at the origin of PBH formation, the dynamical heating and evaporation of clusters, etc. These effects can either boost or suppress the merging rates from clusters and make the whole clustering dynamics a rather complex and model-dependent process, subject to large uncertainties. Invoking clustering is also crucial to evade microlensing limits on stellar masses [76,77] in scenarios with $f_{PBH} = 1$. As an alternative to using uncertain theoretical predictions, one can instead infer an upper limit on the PBH merging rate from LIGO/Virgo observations; see, e.g., Ref. [63]. The merging rate from tidal capture in PBH clusters for an arbitrary mass function is given by [10,63]

$$R^{capt}(m_1, m_2) \equiv \frac{d\tau}{d \ln m_1 d \ln m_2}$$

$$\approx R_{clust} f_{PBH}^2 \times f(m_1) f(m_2)$$

$$\times \frac{(m_1 + m_2)^{10/7}}{(m_1 m_2)^{5/7}} \text{ yr}^{-1} \text{ Gpc}^{-3}, \quad (27)$$

where R_{clust} is an effective parameter encompassing the clustering properties. For $f_{PBH} = 1$ and $R_{clust} \approx 450$, these rates are consistent with the latest LIGO/Virgo observations, for a broad PBH mass function impacted by the transient reduction of the critical threshold of PBH formation at the QCD epoch. As already mentioned, this effect is unavoidable and may have induced a peak around $2.5 M_\odot$ and a bump around $30 M_\odot$ in the PBH mass

function. In this scenario, around one percent of the DM could be made of planetary-mass PBHs around $10^{-5} \, M_\odot$. Like for primordial binaries, we define an effective parameter

$$\tilde{f}_{\mathrm{PBH}} \equiv \left(\frac{R_{\mathrm{clust}}}{450} \right) \times f_{\mathrm{PBH}} f(m_{\mathrm{PBH}}) \qquad (28)$$

representing the DM density fraction at a given mass and per logarithmic mass interval, in the above-mentioned scenario. One then obtains the merging rate for equal-mass binaries,

$$R^{\mathrm{capt}}(m_{\mathrm{PBH}}) = 1.2 \times 10^3 \tilde{f}_{\mathrm{PBH}}^2, \qquad (29)$$

the corresponding source distance D_1^{capt},

$$D_1^{\mathrm{capt}} \approx 58 \text{ Mpc} \times \tilde{f}_{\mathrm{PBH}}^{-2/3}, \qquad (30)$$

and the required experimental strain sensitivity to detect one event per year,

$$h_1^{\mathrm{capt}} \approx 2.7 \times 10^{-22} \tilde{f}_{\mathrm{PBH}}^{2/3} \left(\frac{m_{\mathrm{PBH}}}{M_\odot} \right). \qquad (31)$$

This GW signal is therefore typically lower than that for PBH binaries on planetary-mass scales.

Finally, like for the case of primordial binaries, we have derived the expected limits on $\tilde{f}_{\mathrm{PBH}}$ for a given experimental strain sensitivity,

$$\tilde{f}_{\mathrm{PBH}} \lesssim 2.5 \times 10^4 \left[\frac{h_{\mathrm{det}}}{10^{-20}} \right]^{3/2} \left(\frac{m_{\mathrm{PBH}}}{M_\odot} \right)^{-3/2}. \qquad (32)$$

As an example, if $h_{\mathrm{det}} = 10^{-30}$ and $m_{\mathrm{PBH}} = 10^{-5}$, one gets $\tilde{f}_{\mathrm{PBH}} \lesssim 7 \times 10^{-4}$, which is better than the current microlensing limits. Again, it is more accurate to assume a power sensitivity rather than a strain sensitivity. Doing so, the corresponding limits on $\tilde{f}_{\mathrm{PBH}}$ are represented in our final Fig. 7.

VI. PROBING PBH MERGERS WITH RESONANT EM DETECTORS OF HFGWs

Let us consider GW trains produced during the final inspiraling phase of PBH binaries of different masses and passing through the resonator, and let us analyze the induced EM radiation. For simplicity, we consider a GW propagation collinear with the longitudinal axis of the EM resonator and perpendicular to the outer magnetic field. In this case, the GW can be approximated by a plane wave, i.e., $h_{+,\times} = h_{+,\times}(z,t)$ since the radius of the detector is much smaller than the incoming wavefront for a distant source. Some inclination of the direction of the incoming GW would result in a signal of lower amplitude, since only
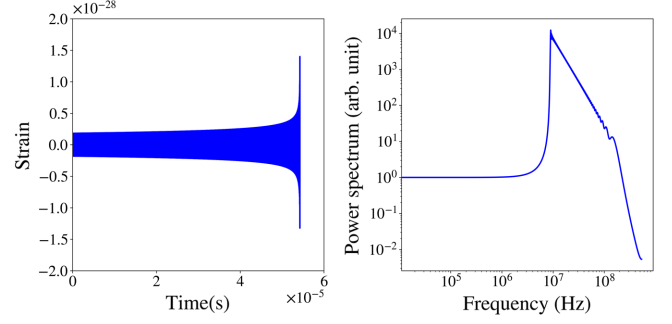

FIG. 2. Left: GW waveform h_+ for the final inspiraling phase of a PBH binary with component masses of $10^{-5} \, M_\odot$, at a distance of 1 Gpc, in the post-Newtonian (4PN) approximation. Right: corresponding GW signal power spectrum.

the component of the GW in the direction of the outer magnetic field contributes to the inverse Gertsenshtein effect. Yet, this ideal case allows to illustrate the physical process and to estimate the expected response of the detector and the output signal. We have computed the typical EM signals for resonators of various shapes. Post-Newtonian time-domain GW waveforms are generated by using the LALSuite library [78], assuming a 4PN approximation. For all of the simulations, we choose a signal sampling frequency that is four times the ISCO frequency [Eq. (16)]. The initial frequency of the signal is set to $f_{\mathrm{ISCO}}/25$. In Fig. 2, we provide an example of the GW waveform produced by the merging of a PBH binary with component masses of $10^{-5} \, M_\odot$ and located at a distance of 1 Gpc. The amplitude of the GW strain at reception, denoted $\mathcal{H}_{\mathrm{GW}}$, is of order 10^{-28} and the signal duration is of order 10^{-5} s.

Then, by using Eq. (13) and solving the forced harmonic oscillator equations (12), we compute the induced EM power for the two designs of resonators. Our results are displayed in Fig. 3, for 1-m long resonators in a 5 T constant magnetic field. The radius of the resonators is set to 5 m, and for the transverse electromagnetic (TEM) coaxial design we consider a 10 cm inner radius. As expected, the induced power increases near the merger. In each case, we have also computed the frequency spectrum of the induced power, which exhibits peaks corresponding to the resonance frequencies, coming from Eqs. (A10) and (A11) in the Appendix. The power rms values are 1.00×10^{-10} W for the TEM resonator and 1.03×10^{-10} W for the TM resonator.

Figure 4 shows the first five proper frequencies of the TEM and TM cavities as a function of their outer radius, within the range 10 cm to 10 m, for a detector of length 1 m. For the TM resonator, these frequencies range from 10 MHz to 10 GHz, while the TEM waveguide can reach higher frequencies for the same detector size. In the case of an outer radius almost equal to the inner one (thin case), the resonance frequencies can be 1 order of magnitude larger
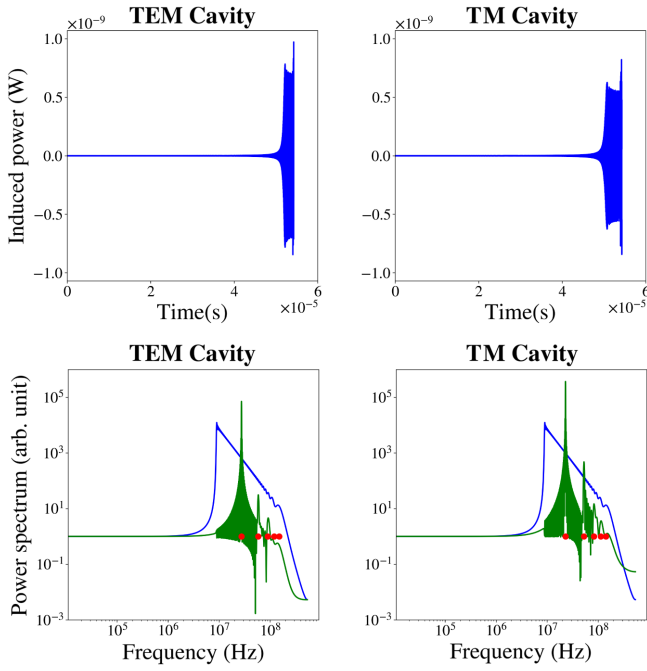
FIG. 3. Top: time evolution of the induced EM power in the two resonators. Bottom: GW signal power spectrum (blue) and induced power spectrum (green). The detectors are 1 m long, in a 5 T constant magnetic field. The outer radius is 5 m, and for the TEM coaxial case the inner radius of 10 cm. The peaks in the power spectrum correspond to the resonance frequencies, represented by the red dots.
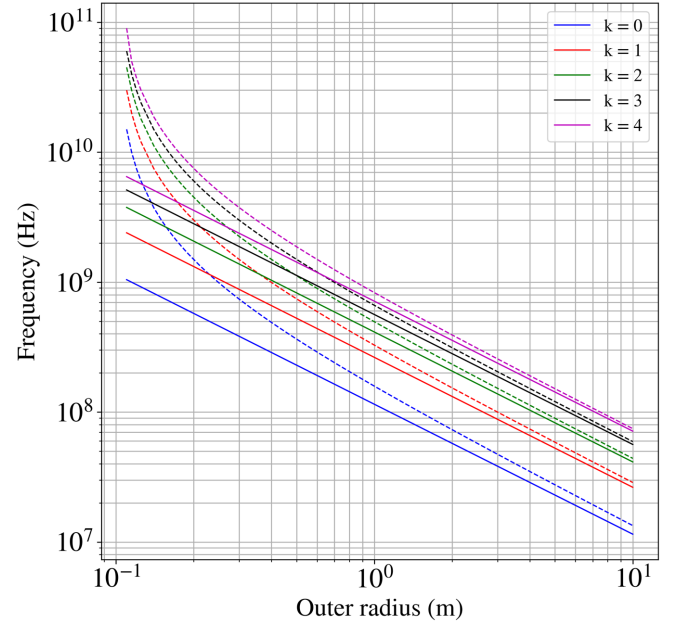

FIG. 4. First five proper frequencies of the cavity (TM resonator, straight lines) and the waveguide (TEM resonator, dashed line) as a function of their outer radius (assuming a length of $L = 1$ m and an inner radius of $R_1 = 0.1$ m for the waveguide).

and the one induced by a range of frequencies inherited from the incoming GW signal. In Fig. 5, the part of the power spectrum induced by the resonance frequencies is overestimated. Indeed, the numerical fast fourier transform
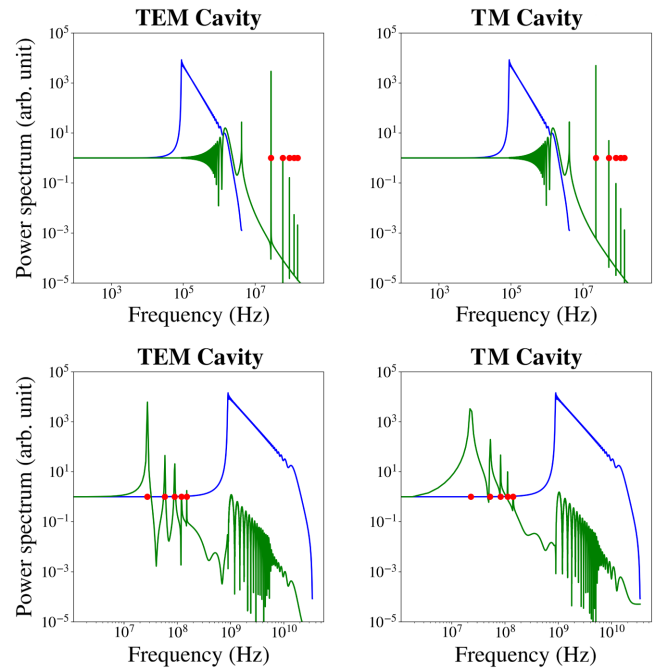
than for a TM resonator. We point out that it would even be possible to use several concentric TEM waveguides to further extend the range of resonance frequencies. Figure 4 therefore illustrates how one could play with the geometry of the experimental setup in order to optimize the detector response to some motivated GW signal. The PBH mass is another parameter to consider. For the same detectors as in Fig. 3, we have simulated the detection of the signal for two additional PBH masses of 10^{-3} and $10^{-7} M_\odot$, and the corresponding power spectra are shown in Fig. 5. For $10^{-3} M_\odot$, the resonance frequencies are higher than the ISCO frequency. The resulting EM power spectrum in the detector exhibits a continuous set of frequencies that matches the incoming GW power spectrum followed by the excitation of the detector resonance frequencies that constitutes the highest values in the induced radiation power spectrum. The continuous set of induced frequencies comes from the particular solution of the forced oscillator (12), while the excitation of the detector resonance frequencies comes from the general solution.

In the $10^{-7} M_\odot$ case, the detector resonance frequencies are lower than the main GW signal frequencies. Therefore, we have a clear separation between the EM power spectrum that is induced by the resonance frequencies of the detector

FIG. 5. Same as the bottom panel of Fig. 3, but for a PBH mass of $10^{-3} M_\odot$ (top panel) and $10^{-7} M_\odot$ (bottom panel). In the first/second case, the GW frequency is below/above the resonance frequencies (represented by the red points) of the detector.

TABLE I.   GW signal duration, maximal strain, ISCO frequency, and the corresponding induced power in the resonant cavity or waveguide, for different values of the PBH mass. The detectors are 1 m long for an outer radius of 5 m. The inner radius in the TEM case is 10 cm. The transverse static magnetic field is set to 5 T. The minimal frequency of the GW waveform signal is set to $f_{\mathrm{ISCO}}/25$. The bandwidth of the resonant frequencies considered is $[2 \times 10^7, 2 \times 10^8]$ Hz.

m_{PBH} ($M_\odot$)	Time (s)	$\mathcal{H}_{\mathrm{GW}}$	f_{ISCO} (Hz)	P_{RMS} TEM (W)	P_{RMS} TM (W)
10^{-3}	5.43×10^{-3}	1.15×10^{-26}	2.20×10^{6}	2.37×10^{-14}	3.19×10^{-14}
10^{-4}	5.43×10^{-4}	1.37×10^{-27}	2.20×10^{7}	2.98×10^{-12}	4.96×10^{-12}
10^{-5}	5.43×10^{-5}	1.40×10^{-28}	2.20×10^{8}	1.00×10^{-10}	1.03×10^{-10}
10^{-6}	5.43×10^{-6}	1.17×10^{-29}	2.20×10^{9}	1.51×10^{-11}	6.31×10^{-12}

(FFT) of the incoming GW leads to a plateau at low frequencies, as shown in Fig. 2. As a result, this plateau will be excited by the proper frequencies of the cavity, leading to an overestimation of this part of the induced power spectrum. We show below how to avoid this numerical limitation.

Finally, we have computed the power in a 1-m long resonator of radius 5 m in a 5 T magnetic field, induced by the merging of PBHs with a broad range of masses. Our results are summarized in Table I. We find that the induced power is maximal for a PBH mass around $10^{-5} M_\odot$, i.e., when the corresponding GW frequency lies within the range of the resonance frequencies. In Fig. 6 we show the rms power as a function of the PBH mass, for the same experimental configuration. In order to do so, we have considered 41 simulated signals of PBH mergers for 61 different PBH masses (i.e., 41 signals per discretization point in mass, and with each of these signals corresponding to different initial frequency ranging from $f_{\mathrm{ISCO}}/30$ to $f_{\mathrm{ISCO}}/10$). Because of the numerical problem at masses beyond $10^{-6} M_\odot$ (poor resolution of the FFT of the GW

signal at low frequencies), we extrapolate our data with the expected behavior that we will develop further in this section. When the GW spectrum covers the fundamental resonance modes of the detector, its response is maximal and this occurs for PBH masses covering 2 orders of magnitude around $10^{-5} M_\odot$.

In addition, we also show in Fig. 6 the rms energy variation inside the cavity, as a function of the PBH mass. The induced energy typically corresponds to millions of photons. It is well above the sensitivity of the ADMX experiment, which has achieved an effective instrumental noise temperature of order $\mathcal{O}(1)$ K at similar frequencies [39,40] and with a similar value of the magnetic field. Further work is however needed in order to more accurately quantify the energy or power sensitivity that could be achieved with a similar technology.

For masses larger than $10^{-4} M_\odot$, the frequencies associated with the GWs are smaller than the proper frequencies of the cavity and so the amplitude of the total solution of Eq. (12) is proportional to the amplitude of the source term, divided by the square of the proper frequencies of the
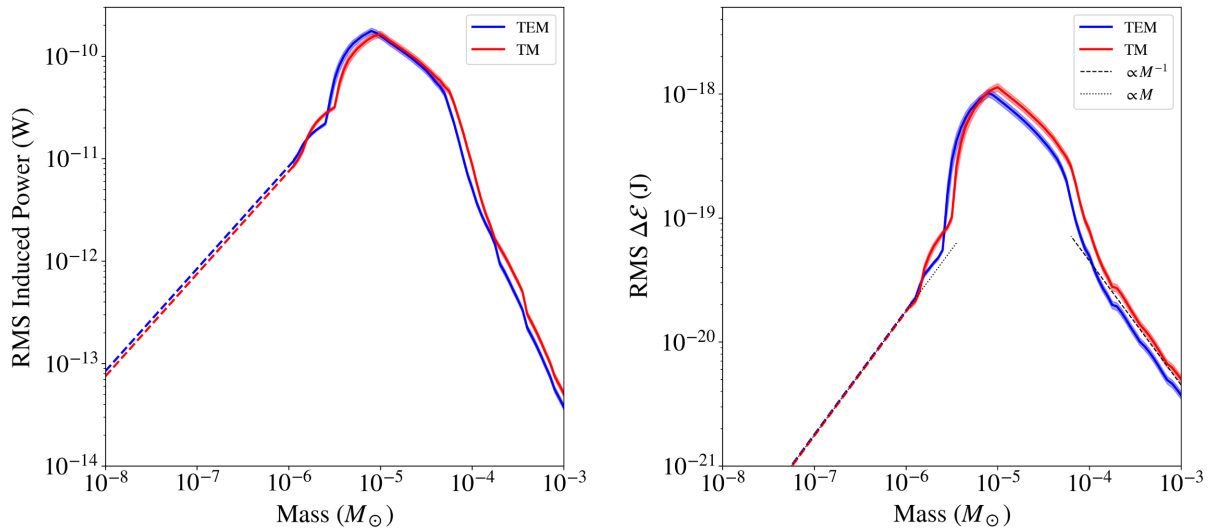

FIG. 6.   rms values of the induced power (left) and energy variation (right) in the TEM (blue) and TM (red) detectors as in Table I, as a function of the PBH mass, for mergers located at a distance of 1 Gpc. The excitation of resonant frequencies boosts the signal in the range between 10^{-6} and $10^{-4} M_\odot$. Below $10^{-6} M_\odot$, we plot as dashed lines the expected behavior due to numerical limitation in our simulations. Asymptotic behavior coming from our analysis is plotted as black dotted lines.
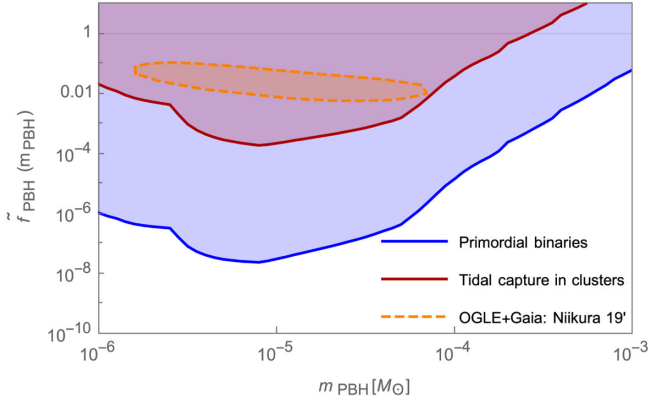
FIG. 7. Expected limits on the effective parameter $\tilde{f}_{PBH}$ corresponding to the dark matter density fraction in PBHs at a given mass and per logarithmic mass interval in the two models described in the text: primordial binaries (blue limit) and tidal capture in halos (red limit). These limits are computed for the proposed experimental designs of EM resonant HFGW detectors, assuming a power sensitivity of 10^{-10} W, achievable with current technology. The orange curve shows the possible abundance of planetary-mass PBHs inferred from recent microlensing observations towards the Galactic bulge [7].

cavity. So the behavior of the particular solution is the same as the source term. From Eq. (10), we know that the source term is proportional to the second time derivative of the strain. On the one hand, the GW strain is proportional to PBH mass [see Eq. (17)]. On the other hand, the maximal GW frequency is inversely proportional to the PBH mass. As a result, the energy released in the detector goes like $1/m_{PBH}$, which explains the linear decreases observed at large mass.

As mentioned earlier, because of a numerical limitation we do not plot the induced energy and rms power for masses smaller than $10^{-6} M_\odot$. Nonetheless, we can extrapolate the expected behavior of the mass dependence. The analysis is the same as in the large-mass regime except that this time it is the proper frequencies of the cavity that are smaller than the frequencies associated with the GWs. Thus, the amplitude of the total solution of Eq. (12) is now proportional to the amplitude of the source term, divided by the square of the GW frequencies. As these frequencies are inversely proportional to the PBH mass, the behavior of the energy released in the detector is m_{PBH}^2 times what it was in the previous case. So the energy variation goes like m_{PBH}. We will show this in a forthcoming paper by using a frequency domain approach.

Finally, we observe that there is no significant difference between the TEM and the TM detectors, highlighting some robustness with respect to the choice of the experimental setup.

As a final step, we have combined our calculations of the PBH merging rates and the induced power as a function of the PBH mass for mergers at a fixed distance of 1 Gpc, in order to forecast limits on the PBH abundance for a fixed

detector sensitivity of 10^{-10} W and a survey of one year. To do so, we have used the calculated values of D_1 for the two binary formation channels. Given that the GW strain is inversely proportional to the distance of the source, the EM power released in the detector is also inversely proportional to the distance; see Eq. (15). Our final results are displayed in Fig. 7. We can clearly see that the resonance plays a role by boosting the detection limits to be as low as $\tilde{f}_{PBH} \lesssim 10^{-8}$ for primordial binaries, and $\tilde{f}_{PBH} \lesssim 10^{-4}$ for tidal capture in clusters. Resonant EM-based HFGW detectors could therefore set unprecedented and independent limits on the abundance of planetary-mass PBHs.

VII. CONCLUSION

The detection of dozens of black hole or neutron star mergers by LIGO/Virgo and, more recently, the plausible observation of a stochastic GW background with pulsar timing arrays (PTAs) by NANOGrav, have revealed the bright future of GW astronomy. LIGO/Virgo probe GW frequencies between 10 and 10^4 Hz and PTAs of 10^{-9} Hz. In the future, ground-based and space detectors like the Einstein Telescope, Cosmic Explorer, and LISA will fill the gap between these two ranges and probe other GW sources like intermediate-mass black hole binaries. On the other side of the GW spectrum, HFGW detectors might be equally interesting and probe cosmological stochastic backgrounds or exotic planetary-mass compact objects like PBHs. Motivated by recent claims that PBHs with a wide mass distribution could explain, among other things, the masses and spins of LIGO/Virgo black holes, the NANOGrav observation, and the dark matter in the Universe, we envisioned their detectability with two designs of resonant EM detectors based on the inverse Gertsenshtein effect and operating at frequencies of order 100 MHz.

The released energy in an EM resonator has been calculated for fourth-order post-Newtonian GW waveforms corresponding to the final inspiraling phase of light PBH binaries. The experimental apparatus consists in either a 1-m long cylindrical resonant cavity (TM) or a conducting waveguide (TEM), together with a static 5 T magnetic field orthogonal to their axis of symmetry. For a 5-m radius resonator or a waveguide of inner radius 0.1 m, we found a typical power variation of order of 10^{-10} W, detectable with present technology. Similar resonant cavities have been already built for axion searches, but their collinear magnetic field prevents the detection of HFGWs. We have also studied the expected signal and its power spectrum for different binary masses. Their merging rates have been estimated for two PBH binary formation channels, in the early Universe or due to tidal capture in dense clusters. The optimal sensitivity is obtained for PBH masses of order $10^{-5} M_\odot$. For the two considered models, we forecast the stringent limits on the PBH abundance that could be set

with such experiments, of order $\tilde{f}_{\text{PBH}} \lesssim 10^{-8}$ and $\tilde{f}_{\text{PBH}} \lesssim 10^{-4}$, respectively. Finally, one should keep in mind that we can tune the parameters of the detector to match the frequency range of highest interest.

Therefore, HFGWs have the ability to set new constraints on the fraction of dark matter made of light PBHs that would be complementary to microlensing limits. In particular, they could be used to distinguish between PBH and planetary origins of recently detected microlensing events towards the Galactic center, suggesting that about one percent of the DM could be made of such objects.

HFGW detectors with similar designs could also be used to detect cosmological stochastic GW backgrounds. Frequencies around 100 MHz are of particular interest in this context, because these are characteristic of GW sources at energies close to the grand unified theory scale, like (p) reheating, oscillons, phase transitions, or evaporating PBHs. In particular, we point out that a strain sensitivity down to $h \sim 10^{-30}$ for achievable TM and TEM detectors is of the order of the typical amplitude of such cosmological backgrounds. Ongoing research focuses on using a frequency analysis of the resonance mechanism to get direct information about the frequency sensitivity of our detector. Another ongoing work is computing the power variation in the detectors generated by a stochastic, almost isotropic GW background. Another future research topic is to characterize the expected experimental noise with such detectors. The results for axion haloscope detection [39,40] could be an interesting starting point.

In summary, resonant electromagnetic HFGW detectors are ideal for probing various aspects of fundamental physics, from early Universe cosmology to exotic compact objects like planetary-mass primordial black holes. Our work contributes to paving the way in this direction and provides strong motivations to start the experimental development of such detectors, with currently available technology.

ACKNOWLEDGMENTS

APPENDIX: DETAILS OF COMPUTATIONS FROM EQ. (7) TO EQS. (12)–(14)

In the Lorenz gauge, an incoming gravitational plane wave can be written, in cylindrical coordinates (t, r, ϕ, z), as

$$h_{rr}(\phi, z, t) = -h_{\phi\phi} = h_+(z, t)\cos(2\phi) + h_\times(z, t)\sin(2\phi),$$
$$h_{r\phi}(\phi, z, t) = -h_+(z, t)\sin(2\phi) + h_\times(z, t)\cos(2\phi),$$

where h_{rr}, $h_{\phi\phi}$, $h_{r\phi}$ are the metric perturbations in the noncoordinate basis $(cdt, dr, rd\phi, dz)$ and h_+ and $h_\times$ are the usual polarizations of the incoming GW in the traceless-transverse gauge.

The incoming GW will interact with the component of the magnetic field that is perpendicular to its direction of propagation. We therefore consider the outer magnetic field along the x direction: $\vec{B}_{\text{ext}}^{(0)} = B_{\text{ext}}^{(0)} \vec{e}_x$. Any component of the magnetic field that would be collinear to the direction of the propagation of the gravitational plane wave, $\vec{B}_{\text{ext}}^{(0)} \approx \vec{e}_z$, does not produce any EM wave through the inverse Gertsenshtein effect. Indeed, since $F^{(0)}{}_{xy} = B_z$, one has that, from Eq. (8),

$$S_{\mu\nu} = -\partial_x(\partial_\mu h_{y\nu} - \partial_\nu h_{y\mu})F^{(0)\,xy} + (x \leftrightarrow y).$$

Each term in the above equation will identically vanish in the case of a plane gravitational wave propagating along the direction of the magnetic field $[h_{+,\times} = h_{+,\times}(z, t)]$.

Let us now assume that our EM resonators are axially symmetric along the z direction and examine Eq. (7) in cylindrical coordinates. The external constant magnetic field along the x direction gives rise to only two components of the zeroth-order electromagnetic tensor,

$$F^{(0)}{}_{rz} = B_{\text{ext}}^{(0)} \sin(\phi),$$
$$F^{(0)}{}_{\phi z} = B_{\text{ext}}^{(0)} \cos(\phi),$$

in the noncoordinate basis $(cdt, dr, rd\phi, dz)$. For an incoming gravitational plane wave interacting with a constant magnetic field along the x direction, Eq. (7) can be written in terms of the induced electric and magnetic fields $\vec{E}^{(1)}$, $\vec{B}^{(1)}$,

$$\left(-\frac{\partial^2}{\partial t^2} + \vec{\Delta}\right)\vec{E}^{(1)} = \vec{S}_E, \tag{A1}$$

$$\left(-\frac{\partial^2}{\partial t^2} + \vec{\Delta}\right)\vec{B}^{(1)} = \vec{S}_B, \tag{A2}$$

with the following source terms:

$$\vec{S}_E^\perp = B_{\text{ext}}^{(0)}\frac{\partial^2 h_+}{\partial t \partial z}\begin{pmatrix} -\sin(\phi) \\ -\cos(\phi) \end{pmatrix} + B_{\text{ext}}^{(0)}\frac{\partial^2 h_\times}{\partial t \partial z}\begin{pmatrix} \cos(\phi) \\ -\sin(\phi) \end{pmatrix}, \tag{A3}$$

$$\vec{S}_B^{\perp} = B_{\text{ext}}^{(0)} \frac{\partial^2 h_+}{\partial z^2} \begin{pmatrix} \cos(\phi) \\ -\sin(\phi) \end{pmatrix} + B_{\text{ext}}^{(0)} \frac{\partial^2 h_\times}{\partial z^2} \begin{pmatrix} \sin(\phi) \\ \cos(\phi) \end{pmatrix}. \tag{A4}$$

Equations (A2) and (A4) lead to Eq. (10) of this paper.

Our earlier demonstration is illustrated here, and indeed the longitudinal components $(E, B)_z^{(1)}$ are not sourced since $S_{E,z} = S_{B,z} = 0$ so that the induced radiation is purely TEM: $(E, B)_z^{(1)} = 0$. In the above equations, $\vec{\Delta}$ is the vector Laplacian operator in cylindrical coordinates, which is given by

$$\vec{\Delta}\,\vec{E} = \begin{pmatrix} \nabla^2 E_r - \frac{E_r}{r^2} - \frac{2}{r^2}\partial_\phi E_\phi \\ \nabla^2 E_\phi - \frac{E_\phi}{r^2} + \frac{2}{r^2}\partial_\phi E_r \\ \nabla^2 E_z \end{pmatrix}, \tag{A5}$$

where ∇^2 is the scalar Laplacian: $\nabla^2 f = \partial_r^2 f + \frac{1}{r}\partial_r f + \frac{1}{r^2}\partial_\phi^2 f + \partial_z^2 f$. Any EM field inside an ideal resonator must verify the boundary conditions along any perfectly conducting surfaces: $\vec{E}_\parallel^{(1)} = \vec{B}_\perp^{(1)} = \vec{0}$. Therefore, any waveguide with two concentric open cylinders will host EM field configurations with $E_z^{(1)}|_{r=R1,R_2} = B_r^{(1)}|_{r=R_1,R_2} = 0$, while a cylindrical conducting cavity will host EM fields satisfying $E_z^{(1)}|_{r=R} = B_r^{(1)}|_{r=R} = 0$ and $E_{r,\phi}^{(1)}|_{z=\pm L/2} = B_z^{(1)}|_{z=\pm L/2} = 0$. The inhomogeneous wave equations (A1)–(A2) can be efficiently solved using spectral methods, i.e., by approximating the unknown field $(\vec{E}, \vec{B})^{(1)}(t, r, \phi, z)$ by a decomposition over a basis of orthogonal functions that satisfy the above-mentioned boundary conditions. Here, a natural choice of such a basis is given by the following set of cylindrical harmonics (omitting the useless longitudinal component ψ_{kmn}^z):

$$\psi_{kmn}^r = C_{kmn} \cdot \mathcal{R}_{km}(r) \cdot \begin{Bmatrix} \cos \\ \sin \end{Bmatrix}(m\phi) \cdot \begin{Bmatrix} \cos \\ \sin \end{Bmatrix}\left(\frac{2\pi n z}{L}\right), \tag{A6}$$

$$\psi_{kmn}^\phi = \mp C_{kmn} \cdot \mathcal{R}_{km}(r) \cdot \begin{Bmatrix} \sin \\ \cos \end{Bmatrix}(m\phi) \cdot \begin{Bmatrix} \cos \\ \sin \end{Bmatrix}\left(\frac{2\pi n z}{L}\right), \tag{A7}$$

where C_{kmn} are normalization coefficients and the radial eigenfunctions $\mathcal{R}_{km}(r)$ are such that the boundary conditions are satisfied. This is the case when

$$\mathcal{R}_{km}(r) = A_k \cdot J_{m-1}(\alpha_k \cdot r) + Y_{m-1}(\alpha_k \cdot r) \tag{A8}$$

$$= J_{m-1}(\alpha_k \cdot r) \tag{A9}$$

for the waveguide and the cavity, respectively. In the above equation, $J_n(r), Y_n(r)$ are Bessel functions of the first and second kind, respectively, and the constants A_{km} and α_k are solutions of the system

$$A_k \cdot J_{m-1}(\alpha_k \cdot R_{1,2}) + Y_{m-1}(\alpha_k \cdot R_{1,2}) = 0 \tag{A10}$$

for the case of the waveguide with two open conducting cylinders and

$$J_{m-1}(\alpha_k \cdot R) = 0 \tag{A11}$$

in the case of the cylindrical cavity.

The cylindrical harmonics $(\vec{\psi}_{kmn})^T = (\psi_{kmn}^r, \psi_{kmn}^\phi, \psi_{kmn}^z)$ are eigenfunctions of the vector Laplacian operator $\vec{\Delta}$ in cylindrical coordinates with the following eigenvalues:

$$\vec{\Delta}\vec{\psi}_{kmn} = -\left(\alpha_k^2 + \frac{4\pi^2 n^2}{L^2}\right)\vec{\psi}_{kmn} = -\Omega_{kn}^2\vec{\psi}_{kmn}. \tag{A12}$$

These eigenfunctions $\psi_{kmn}^{r,\phi}$ constitute a complete orthonormal set with the scalar product

$$(f, g) = \int_{R_1(0)}^{R_2(R)} \int_0^{2\pi} \int_{-L/2}^{L/2} f(r, \phi, z)g(r, \phi, z) r.dr.d\phi.dz,$$

where the different bounds of the integral over the radius correspond to the case of a waveguide or a cavity.

Moving back to Eqs. (A1)–(A2), one can use a truncated expansion in this basis as an approximation of the unknown field. For instance, let us set

$$B_{r,\phi}^{(1)}(t, r, \phi, z) \approx \sum_{k,m,n} \hat{b}_{k,m,n}^{r,\phi}(t) \cdot \psi_{kmn}^{r,\phi}(r, \phi, z), \tag{A13}$$

with

$$\hat{b}_{k,m,n}^{r,\phi}(t) = (B_{r,\phi}^{(1)}, \psi_{k,m,n}^{r,\phi}),$$

so that the inhomogeneous wave equation (A2) now reduces to a harmonic oscillator ordinary differential equation for each mode $\hat{b}_{k,m,n}^{r,\phi}(t)$ [Eq. (12) in the paper],

$$\frac{d^2\hat{b}_{k,m,n}^{r,\phi}}{dt^2} + \Omega_{kn}^2 \hat{b}_{k,m,n}^{r,\phi} = \hat{s}_{k,m,n}^{r,\phi}(t), \tag{A14}$$

where $\hat{s}_{k,m,n}^{r,\phi}(t)$ are the spectral coefficients of the source $S_B^{r,\phi}$:

$$S_B^{r,\phi}(t, r, \phi, z) \approx \sum_{k,m,n} \hat{s}_{k,m,n}^{r,\phi}(t) \cdot \psi_{kmn}^{r,\phi}(r, \phi, z).$$

In this approach, each mode $\hat{b}_{k,m,n}^{r,\phi}(t)$ that composes the induced magnetic field $\vec{B}^{(1)}$ behaves as a harmonic oscillator driven by the corresponding mode of the source $\hat{s}_{k,m,n}^{r,\phi}$.

The general solution of such a system describes a resonance process through a superposition of oscillations at proper frequency Ω_{kn} and a particular solution of the inhomogeneous equation. The latter can be easily obtained in the Fourier space. Since the source of the induced magnetic field is directly related to the second derivative of the metric perturbation, resonance will be achieved when the incoming GWs share some common frequencies with the coaxial detector, as we have seen in the main text.

Fortunately, there are some simplifications allowing to restrict to specific modes of the cylindrical harmonic decomposition of the induced EM fields $(\vec{E}^{(1)}, \vec{B}^{(1)})$. First, in the case of a plane gravitational wave with a direction of propagation perpendicular to that of the outer magnetic field $\vec{B}^{(0)}$, the source terms are given by Eqs. (A3)–(A4) and therefore the induced EM fields will only have an azimuthal mode number equal to one: $m = 1$. Second, if one focuses on the detection of the induced EM energy inside the resonator, it suffices to consider that the components of the induced magnetic fields that are in the same direction as the outer strong magnetic field. Indeed, the EM radiation that is induced in the resonators will modify their EM energy content. The total electromagnetic energy $\mathcal{E}$ inside the waveguide is given by the classical formula

$$\mathcal{E} = \frac{1}{2} \int_V \left(\epsilon_0 \|\vec{E}\|^2 + \frac{\|\vec{B}\|^2}{\mu_0} \right) dV,$$

where V is the volume of the waveguide. The dominant contribution to the energy variation $\Delta\mathcal{E}$ is given by the coupling between the external magnetic field $\vec{B}^{(0)}$ and the induced one $\vec{B}^{(1)}$,

$$\Delta\mathcal{E} = E_{\text{tot}} - E^{(0)} \approx \frac{1}{\mu_0} \int_V (\vec{B}^{(0)} \cdot \vec{B}^{(1)}) dV, \quad (A15)$$

neglecting the terms in $\|\vec{E}^{(1)}\|^2$ and $\|\vec{B}^{(1)}\|^2$. Since we have assumed here that the external magnetic field lies in the x direction, one only needs to compute

$$B_x^{(1)} = B_r^{(1)} \cos\phi - B_\phi^{(1)} \sin\phi$$

from Eqs. (A2) and (A4). In the case of an incoming plane GW orthogonal to the outer magnetic field, only the modes with $m = 1$ (such that $B_r^{(1)} \approx \cos\phi$ and $B_\phi^{(1)} \approx -\sin\phi$; see above) and $n = 0$, i.e., constant in the z direction, will give a nonvanishing contribution to the integral over the volume in the computation of the energy. The important terms are therefore sourced by Eq. (14),

$$\hat{s}_{k,1,0}^{r,\phi}(z,t) = \pi B_0 L^2 \mathcal{I}_k \int_{-L/2}^{L/2} \frac{\partial^2 h_+(z,t)}{\partial z^2} dz, \quad (A16)$$

with the dimensionless quantity $\mathcal{I}_k$ given by

$$\mathcal{I}_k = \int_{r_1(0)}^{r_2(R/L)} \mathcal{R}_{k,1}(L\rho)\rho \, d\rho, \quad (A17)$$

with $\rho = r/L$, $r_{1,2} = R_{1,2}/L$ and for a magnetic field along the x direction.

In summary, the energy variation at the leading order is given by Eq. (13),

$$\Delta\mathcal{E} \approx \frac{2\pi B_0}{\mu_0} \cdot \sum_k \mathcal{I}_k \hat{b}_{k,1,0}(t), \quad (A18)$$

with $\hat{b}_{k,1,0}(t) = \hat{b}_{k,1,0}^r(t) + \hat{b}_{k,1,0}^\phi(t) = 2\hat{b}_{k,1,0}^{r,\phi}(t)$. The modes $\hat{b}_{k,1,0}(t)$ are solutions of the forced harmonic oscillator equation (A14) with a source term given by (twice) Eq. (A16). This completes the detailed explanation of how to obtain Eqs. (12)–(14).

[1] A. Einstein, *Sitzungsberichte der Königlich Preußischen Akademie der Wissenschaften*, Vol. 688 (Berlin, 1916).

[2] A. Einstein, *Sitzungsberichte der Königlich Preußischen Akademie der Wissenschaften*, Vol. 154 (Berlin, 1918).

[3] B. P. Abbott, R. Abbott, T. D. Abbott *et al.*, Phys. Rev. Lett. **116**, 061102 (2016).

[4] M. Gertsenshtein, J. Exp. Theor. Phys. **14**, 113 (1960), http://www.jetp.ac.ru/cgi-bin/e/index/e/14/1/p84?a=list.

[5] N. Aggarwal, O. D. Aguiar, A. Bauswein, G. Cella, S. Clesse *et al.*, arXiv:2011.12414.

[6] A. Füzfa, Devices for the directional emission and reception of gravitational waves, Patents PCT/EP2018/086758, PCT/EP2018/086760.

[7] H. Niikura, M. Takada, S. Yokoyama, T. Sumi, and S. Masaki, Phys. Rev. D **99**, 083503 (2019).

[8] P. Mróz, A. Udalski, J. Skowron, R. Poleski, S. Kozłowski, M. K. Szymański, I. Soszyński, Ł. Wyrzykowski, P. Pietrukowicz, K. Ulaczyk, D. Skowron, and M. Pawlak, Nature (London) **548**, 183 (2017).

[9] S. Bird, I. Cholis, J. B. Muñoz, Y. Ali-Haïmoud, M. Kamionkowski, E. D. Kovetz, A. Raccanelli, and A. G. Riess, Phys. Rev. Lett. **116**, 201301 (2016).

[10] S. Clesse and J. García-Bellido, Phys. Dark Universe **15**, 142 (2017).

[11] M. Sasaki, T. Suyama, T. Tanaka, and S. Yokoyama, Phys. Rev. Lett. **117**, 061101 (2016).

[12] B. Carr, S. Clesse, J. García-Bellido, and F. Kühnel, Phys. Dark Universe **31**, 100755 (2021).

[13] J. Weber, Phys. Rev. **117**, 306 (1960).

[14] D. Boccaletti, V. De Sabbata, P. Fortini, and C. Gualdi, Il Nuovo Cimento B **70**, 129 (1970).

[15] W. K. De Logi and A. R. Mickelson, Phys. Rev. D **16**, 2915 (1977).

[16] Y. B. Zeldovich, Sov. Phys. JETP **38**, 652 (1974), http://jetp .ac.ru/cgi-bin/dn/e_038_04_0652.pdf.

[17] L. P. Grishchuk and M. V. Sazhin, Zh. Eksp. Teor. Fiz. **65**, 441 (1973), http://jetp.ac.ru/cgi-bin/dn/e_038_02_0215 .pdf.

[18] L. P. Grishchuk and M. V. Sazhin, Zh. Eksp. Teor. Fiz. **68**, 1569 (1975), http://jetp.ac.ru/cgi-bin/dn/e_038_02_ 0215.pdf.

[19] L. P. Grishchuk, Sov. Phys.-Usp. **20**, 319 (1977).

[20] L. P. Grishchuk, arXiv:gr-qc/0306013.

[21] V. B. Braginskii and M. B. Menskii, JETP Letters, Technical Report No. 11, Moscow State Univ., 1971.

[22] V. B. Braginskii, L. P. Grishchuk, A. G. Doroshkevich, Y. B. Zel'dovich, I. D. Novikov, and M. V. Sazhin, Zhurnal Eksperimental'noi i Teoreticheskoi Fiziki, Technical Report No. 5, Moscow State Univ., 1973.

[23] F. Pegoraro, L. A. Radicati, P. Bernard, and E. Picasso, Phys. Lett. **68A**, 165 (1978).

[24] F. Pegoraro, E. Picasso, and L. A. Radicati, J. Phys. A **11**, 1949 (1978).

[25] C. M. Caves, Phys. Lett. **80B**, 323 (1979).

[26] U. H. Gerlach, Phys. Rev. D **46**, 1239 (1992).

[27] A. M. Cruise, Mon. Not. R. Astron. Soc. **204**, 485 (1983).

[28] R. Ballantini, P. Bernard, E. Chiaveri, A. Chincarini, G. Gemme, R. Losito, R. Parodi, and E. Picasso, Classical Quantum Gravity **20**, 3505 (2003).

[29] A. Ejlli, D. Ejlli, A. M. Cruise, G. Pisano, and H. Grote, Eur. Phys. J. C **79**, 1 (2019).

[30] J. Bentley, P. Jones, D. Martynov, A. Freise, and H. Miao, Phys. Rev. D **99**, 102001 (2019).

[31] A. Arvanitaki and A. A. Geraci, Phys. Rev. Lett. **110**, 071105 (2013).

[32] N. Aggarwal, G. P. Winstone, M. Teo, M. Baryakhtar, S. L. Larson, V. Kalogera, and A. A. Geraci, arXiv:2010.13157.

[33] A. Ito, T. Ikeda, K. Miuchi, and J. Soda, Eur. Phys. J. C **80**, 179 (2020).

[34] M. Goryachev and M. E. Tobar, Phys. Rev. D **90**, 102005 (2014).

[35] A. Füzfa, Phys. Rev. D **93**, 024014 (2016).

[36] R. C. Tolman, P. Ehrenfest, and B. Podolsky, Phys. Rev. **37**, 602 (1931).

[37] D. Rätzel, M. Wilkens, and R. Menzel, New J. Phys. **18**, 023009 (2016).

[38] T. Meng-Xi, L. Fang-Yu, and L. Jun, Acta Physica Sinica (Overseas Edition) **6**, 161 (1997).

[39] S. J. Asztalos, G. Carosi, C. Hagmann, D. Kinion, K. Van Bibber, M. Hotz, L. J. Rosenberg, G. Rybka, J. Hoskins, J. Hwang, P. Sikivie, D. B. Tanner, R. Bradley, and J. Clarke, Phys. Rev. Lett. **104**, 041301 (2010).

[40] N. Du, N. Force, R. Khatiwada, E. Lentz *et al.* (ADMX Collaboration), Phys. Rev. Lett. **120**, 151301 (2018).

[41] Y. Choquet-Bruhat, *General Relativity and the Einstein Equations*, Oxford Mathematical Monographs (OUP Oxford, New York, 2009).

[42] T. Nakamura, M. Sasaki, T. Tanaka, and K. S. Thorne, Astrophys. J. Lett. **487**, L139 (1997).

[43] A. Kashlinsky, Astrophys. J. Lett. **823**, L25 (2016).

[44] C. Kouvaris, P. Tinyakov, and M. H. Tytgat, Phys. Rev. Lett. **121**, 221102 (2018).

[45] B. Dasgupta, R. Laha, and A. Ray, Phys. Rev. Lett. **126**, 141105 (2021).

[46] C. T. Byrnes, M. Hindmarsh, S. Young, and M. R. S. Hawkins, J. Cosmol. Astropart. Phys. 08 (2018) 041.

[47] S. Clesse and J. García-Bellido, Phys. Dark Universe **22**, 137 (2018).

[48] M. R. Hawkins, Astron. Astrophys. **633**, A107 (2020).

[49] S. Bhatiani, X. Dai, and E. Guerras, Astrophys. J. **885**, 77 (2019).

[50] Z. Arzoumanian *et al.* (NANOGrav Collaboration), Astrophys. J. Lett. **905**, L34 (2020).

[51] G. Domènech and S. Pi, arXiv:2010.03976.

[52] V. De Luca, G. Franciolini, and A. Riotto, Phys. Rev. Lett. **126**, 041303 (2021).

[53] V. Vaskonen and H. Veermäe, Phys. Rev. Lett. **126**, 051303 (2021).

[54] K. Kohri and T. Terada, Phys. Lett. B **813**, 136040 (2021).

[55] S. Wang, T. Terada, and K. Kohri, Phys. Rev. D **99**, 103531 (2019).

[56] S. Wang, T. Terada, and K. Kohri, Phys. Rev. D **99**, 103531(E) (2019).

[57] J. M. Antelis, J. M. Hernández, and C. Moreno, J. Phys. Conf. Ser. **1030**, 012005 (2018).

[58] B. Kocsis, T. Suyama, T. Tanaka, and S. Yokoyama, Astrophys. J. **854**, 41 (2018).

[59] M. Raidal, C. Spethmann, V. Vaskonen, and H. Veermäe, J. Cosmol. Astropart. Phys. 02 (2019) 018.

[60] A. D. Gow, C. T. Byrnes, A. Hall, and J. A. Peacock, J. Cosmol. Astropart. Phys. 01 (2020) 031.

[61] L. Liu, Z. K. Guo, and R. G. Cai, Phys. Rev. D **99**, 063523(E) (2019).

[62] V. Vaskonen and H. Veermäe, Phys. Rev. D **101**, 043015 (2020).

[63] S. Clesse and J. Garcia-Bellido, arXiv:2007.06481.

[64] C. Boehm, A. Kobakhidze, C. A. O'Hare, Z. S. Picker, and M. Sakellariadou, J. Cosmol. Astropart. Phys. 03 (2021) 078.

[65] J. R. Chisholm, Phys. Rev. D **73**, 083504 (2006).

[66] J. R. Chisholm, Phys. Rev. D **84**, 124031 (2011).

[67] K. M. Belotsky, V. I. Dokuchaev, Y. N. Eroshenko, E. A. Esipova, M. Y. Khlopov, L. A. Khromykh, A. A. Kirillov, V. V. Nikulin, S. G. Rubin, and I. V. Svadkovsky, Eur. Phys. J. C **79**, 246 (2019).

[68] B. Carr and J. Silk, Mon. Not. R. Astron. Soc. **478**, 3756 (2018).

[69] T. Suyama and S. Yokoyama, Prog. Theor. Exp. Phys. **2019,** 103E02 (2019).

[70] A. M. Dizgah, G. Franciolini, and A. Riotto, J. Cosmol. Astropart. Phys. 11 (2019) 001.

[71] T. Matsubara, T. Terada, K. Kohri, and S. Yokoyama, Phys. Rev. D **100,** 123544 (2019).

[72] S. Young and C. T. Byrnes, J. Cosmol. Astropart. Phys. 03 (2020) 004.

[73] N. Padilla, J. Magana, J. Sureda, and I. J. Araya, Mon. Not. R. Astron. Soc. **504,** 3139 (2021)..

[74] V. De Luca, V. Desjacques, G. Franciolini, and A. Riotto, J. Cosmol. Astropart. Phys. 11 (2020) 028.

[75] K. Jedamzik, J. Cosmol. Astropart. Phys. 09 (2020) 022.

[76] J. García-Bellido and S. Clesse, Phys. Dark Universe **19,** 144 (2018).

[77] J. Calcino, J. Garcia-Bellido, and T. M. Davis, Mon. Not. R. Astron. Soc. **479,** 2889 (2018).

[78] LIGO Scientific Collaboration, LIGO Algorithm Library-LALSuite, free software (GPL) (2018), https://doi.org/10.7935/GT1W-FZ16.